

Oxygen vacancies in SrTiO₃ thin films at finite temperatures: A first-principles study

Zizhen Zhou and Dewei Chu

School of Materials Science and Engineering, UNSW Australia, Sydney NSW 2052, Australia

Claudio Cazorla*

Departament de Física, Universitat Politècnica de Catalunya, Campus Nord B4-B5, E-08034 Barcelona, Spain

Epitaxially grown SrTiO₃ (STO) thin films are material enablers for a number of critical energy-conversion and information-storage technologies like electrochemical electrode coatings, solid oxide fuel cells and random access memories. Oxygen vacancies (V_O), on the other hand, are key defects to understand and tailor many of the unique functionalities realized in oxide perovskite thin films. Here, we present a comprehensive and technically sound *ab initio* description of V_O in epitaxially strained (001) STO thin films. The novelty of our first-principles study lies in the incorporation of lattice thermal excitations on the formation energy and diffusion properties of V_O over wide epitaxial strain conditions ($-4 \leq \eta \leq +4\%$). We found that thermal lattice excitations are necessary to obtain a satisfactory agreement between first-principles calculations and the available experimental data on the formation energy of V_O for STO thin films. Furthermore, it is shown that thermal lattice excitations noticeably affect the energy barriers for oxygen ion diffusion, which strongly depend on η and are significantly reduced (increased) under tensile (compressive) strain, also in consistent agreement with the experimental observations. The present work demonstrates that for a realistic theoretical description of oxygen vacancies in oxide perovskite thin films is necessary to consider lattice thermal excitations, thus going beyond standard zero-temperature *ab initio* approaches.

I. INTRODUCTION

Crystalline defects, namely, deviations from the ideal and translationally invariant arrangement of atoms in crystals, are ubiquitous in real solids. Fortunately, the presence of crystalline defects is desirable for enhancing the functionality of many materials [1–4]. A quintessential example of a functional type of crystalline defect are oxygen vacancies (V_O). Oxygen vacancies, for instance, can drastically boost the catalytic activity of transition metal oxide (TMO) surfaces by providing abundant reactive sites as well as highly mobile charges [4–6]. The magnetic properties of TMO also can be altered substantially by changing their oxygen content since the exchange interactions between transition metal ions typically are sustained by O atoms [7–9]. Moreover, the presence of V_O enables ionic conductivity in perovskite-based solid solutions that are employed in critical electrochemical applications like solid oxide fuel and electrolysis cells [10, 11]. Consequently, the functionality of TMO materials can be tailored and finely tuned through their stoichiometry.

Another functionality design strategy that has proved very successful for TMO materials is strain engineering [12–14]. Strain engineering consists in growing epitaxial thin films on top of substrates that present a lattice parameter mismatch, η . Either compressive or tensile biaxial stress can thus be introduced in the thin film upon the condition of coherent elastic coupling with the substrate. The ferroelectric [14–18], magnetic [8, 19], optical [20, 21] and catalytic [12, 21] properties of TMO thin films can be drastically changed by strain engineering due

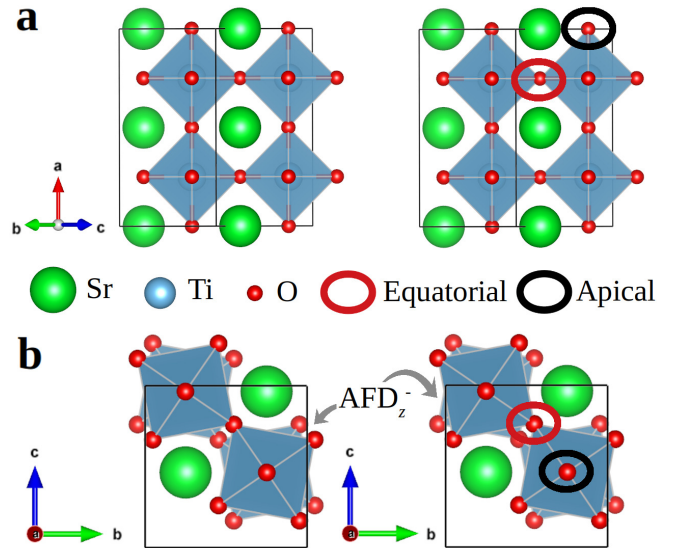


FIG. 1: Representation of the 20-atoms simulation cell employed for the simulation of stoichiometric and epitaxially strained (001) SrTiO₃ thin films. Different views of the simulation cell are represented in **a** and **b** along with the typical antiphase out-of-plane oxygen octahedral antiferrodistortive distortions (AFD_z⁻) found in (001) SrTiO₃ thin films. The positions of generic equatorial and apical oxygen ions are also indicated in the figure.

to the existing strong couplings between their structural and electronic degrees of freedom.

Recently, it has been realized that strain engineering also can be used to tune the formation and diffusion of oxygen vacancies in oxide thin films, and that such a combined η -V_O physico-chemical approach represents a

*Corresponding Author

very promising technique for engineering new materials [22–25]. An illustrative example of the rich interplay between epitaxial strain and oxygen vacancies, which in turn may enormously influence the prevalent orbital and structural order parameters, is provided by the archetypal oxide perovskite SrTiO₃ (STO).

Bulk STO is a quantum paraelectric crystal with an ideal cubic perovskite structure and high dielectric constant that strongly depends on temperature [26]. Bulk STO is broadly used as a substrate in which to grow epitaxial perovskite thin films of high quality and as a key component of oxide heterostructures that exhibit fundamentally intriguing physical behaviour like LaTiO₃/STO bilayers (e.g., formation of a 2D electron gas at the interface) [27] and PbTiO₃/STO superlattices (e.g., emergence of polar vortices) [28]. At room temperature, STO epitaxial thin films may display in-plane ferroelectricity upon biaxial tensile stress [29] and out-of-plane ferroelectricity upon biaxial compressive stress [30]. Within a certain range of biaxial compressive stress, antiferrodistortive (AFD) oxygen octahedra rotations are observed to coexist with out-of-plane electric polarization [30], thus pointing to the presence of unusual cooperative couplings between such normally opposing order parameters [31].

The interplay between oxygen vacancies and biaxial stress in STO thin films is very rich and appears to be further enhanced by the coexistence of AFD distortions and ferroelectricity [32, 33]. Experimentally, it has been shown that both compressive and tensile biaxial strains significantly decrease the formation enthalpy of oxygen vacancies in STO thin films (e.g., by $\sim 10\%$ for $|\eta| \sim 1\%$) [34]. This behaviour is different from zero-temperature first-principles (also referred to as *ab initio*) results obtained for other prototype oxide perovskites like BaTiO₃ and PbTiO₃, which indicate that compressive (tensile) biaxial stress typically depletes (promotes) the formation of V_O [35, 36]. Meanwhile, atomic force microscopy experiments have shown that tensile biaxial strain produces a substantial increase in the mobility of oxygen vacancies whereas small compressive biaxial strain produces an incipient V_O diffusion depletion [37]. These latter experimental observations appear to be in partial disagreement with previous zero-temperature first-principles studies in which it has been concluded that both tensile and compressive biaxial strains tend to promote the migration of oxygen vacancies in STO thin films [38, 39].

First-principles calculations have been used to rationalize the atomistic mechanisms of strain-mediated formation of oxygen vacancies for a number of oxide perovskite thin films like BaTiO₃ [35], PbTiO₃ [36], CaMnO₃ [40], and SrCoO₃ [25, 41]. As previously mentioned, zero-temperature *ab initio* calculations, which by definition neglect thermal excitations, mostly agree in that the formation of V_O is strongly enhanced (reduced) by tensile (compressive) epitaxial strain. This behaviour has been explained in terms of an effective decrease in the electrostatic repulsive interactions between electronically

reduced TM ions, which follows from an increase in the average distance between them [40]. However, the non-monotonic peak-like η -dependence of the V_O formation enthalpy that has been measured for biaxially strained STO thin films [34] cannot be satisfactorily explained in terms of such electrostatic arguments (as otherwise the formation energy of oxygen vacancies should increase, rather than decrease, under compressive η conditions). Likewise, the partial disagreements between theory and experiments on the diffusion properties of oxygen vacancies [37–39] appear to suggest that some key elements might be missing in the *ab initio* calculations [41].

Here, we present a comprehensive first-principles study on the formation energy and migration of oxygen vacancies in epitaxially strained (001) STO thin films that explicitly incorporates lattice thermal effects. This improvement is achieved by means of quasi-harmonic free energy approaches and *ab initio* molecular dynamics (AIMD) simulations (Sec.II). In particular, we compare the formation energies and energy barriers for oxygen diffusion estimated both at zero temperature and $T \neq 0$ conditions, and discuss their agreement with the available experimental data. It is found that thermal lattice excitations are necessary to qualitatively reproduce the measured dependence of the V_O formation energy on biaxial stress. Thermal lattice excitations are also found to enhance V_O migration by reducing the involved energy barriers in about 40%. In agreement with the experiments, the diffusion coefficient of oxygen ions is found to substantially increase under tensile biaxial stress and to decrease under compressive biaxial stress. The present works evidences the need to use finite-temperature first-principles methods to rationalize the experimental findings on off-stoichiometric oxide perovskite thin films and to guide the engineering of new functional materials based on combined physico-chemical approaches.

II. COMPUTATIONAL METHODS

A. General technical details

We used the generalised gradient approximation to density functional theory (DFT) due to Perdew, Burke, and Ernzerhof (GGA-PBE) [42] as is implemented in the VASP software [43]. A “Hubbard- U ” scheme [44] was employed for a better treatment of Ti 3*d* electrons ($U_{\text{eff}} = 2.0$ eV). We used the “projector augmented wave” method [45] to represent the ionic cores and considered the following electronic states as valence: Sr 4*s*, 4*p* and 5*s*; Ti 3*p*, 4*s* and 3*d*; O 2*s* and 2*p*. Wave functions were represented in a plane-wave basis truncated at 650 eV. For simulation of the stoichiometric systems, we employed a 20-atoms simulation cell that allows to reproduce the usual ferroelectric and O₆ antiferrodistortive (AFD) distortions in perovskite oxides [8, 16] (Fig.1). Off-stoichiometric systems containing oxygen vacancies, V_O, were generated by removing oxygen atoms from ei-

ther equatorial (Eq) or apical (Ap) positions (Fig.1). Simulation cells of different sizes were considered in order to quantify the effects of oxygen vacancy concentration on the obtained formation energy results. In particular, the following compositions were investigated: $\text{Sr}_4\text{Ti}_4\text{O}_{11}$ (or, equivalently, $\text{SrTiO}_{2.75}$), $\text{Sr}_8\text{Ti}_8\text{O}_{23}$ ($\text{SrTiO}_{2.88}$), and $\text{Sr}_{16}\text{Ti}_{16}\text{O}_{47}$ ($\text{SrTiO}_{2.94}$). For integrations within the Brillouin zone (BZ), we used a Γ -centered \mathbf{k} -point grid of $6 \times 8 \times 8$ for the 20-atoms simulation cell and scaled it conveniently to maintain an equivalent \mathbf{k} -point density for the rest of cases. All oxygen vacancies were assumed to be neutrally charged and non-magnetic (V_{O}) since this configuration has been shown to render the lowest energy for bulk off-stoichiometric SrTiO_3 in previous DFT studies [9, 46].

The geometry relaxations of epitaxially strained (001) SrTiO_3 and $\text{SrTiO}_{3-\delta}$ were carried out by using a conjugated gradient algorithm that allows to change the simulation-cell volume and atomic positions while constraining the length and orientation of the two in-plane lattice vectors (that is, $|a| = |b|$ and $\gamma = 90^\circ$). Periodic boundary conditions were applied along the three lattice-vector directions, thus the influence of surface and interface effects were systematically neglected in our simulations. This type of calculations are known as “strained-bulk” geometry relaxations and typically are considered to be a good approximation for thin films presenting thicknesses of at least few nanometers (that is, for which surface and interface effects can be safely disregarded) [8, 16]. The simulated systems were assumed to be elastically coupled to a substrate thus the existence of possible stress relaxation mechanisms in the thin films were also neglected. The geometry relaxations were stopped when the forces on the ions were smaller than $0.01 \text{ eV}/\text{\AA}$. By using these parameters we obtained zero-temperature energies that were converged to within 0.5 meV per formula unit.

The electric polarization of stoichiometric and off-stoichiometric (001) SrTiO_3 thin films were estimated with the Born effective charges method [8, 16]. In this approach, the electric polarization is calculated via the formula:

$$P_\alpha = \frac{1}{\Omega} \sum_{\kappa\beta} Z_{\kappa\beta\alpha}^* u_{\kappa\beta}, \quad (1)$$

where Ω is the volume of the cell, κ runs over all the atoms, $\alpha, \beta = x, y, z$ represent the Cartesian directions, \mathbf{u}_κ is the displacement vector of the κ -th atom as referred to a non-polar reference phase, and \mathbf{Z}_κ^* the Born effective charge tensor calculated for a non-polar reference state. It is worth noting that the presence of oxygen vacancies typically induced a notable reduction in the energy band gap of off-stoichiometric systems, which in some cases led to the appearance of metallic states. Consequently, estimation of the electric polarization with the more accomplished and accurate Berry phase formalism was not possible for all the analyzed compositions and thus we

opted for systematically using the approximate Born effective charges method [8, 47].

B. Phonon calculations

To estimate phonon frequencies we employed the “small-displacement” approach [48], in which the force-constant matrix of the crystal is calculated in real space by considering the proportionality between the atomic displacements and forces when the former are sufficiently small (in the present study this condition was satisfied for atomic displacements of 0.02 \AA). Large supercells containing 160 atoms were employed to guarantee that the elements of the force-constant matrix presented practically negligible values at the largest atomic separations. We used a dense \mathbf{k} -point grid of $3 \times 3 \times 3$ for the calculation of the atomic forces with VASP. The computation of the nonlocal parts of the pseudopotential contributions were performed in reciprocal space in order to maximise the numerical accuracy. Once a force-constant matrix was determined, we Fourier transformed it to obtain the phonon frequencies for any arbitrary \mathbf{k} -point in the first BZ. This latter step was performed with the PHON code [48], in which the translational invariance of the system is exploited to ensure that the three acoustic branches are exactly zero at the Γ point. Central differences for the atomic forces, that is, both positive and negative atomic displacements, were considered. A complete phonon calculation involved the evaluation of atomic forces for 120 (114) different stoichiometric (off-stoichiometric) configurations with the technical parameters just described. In order to accurately compute $F_{\text{vac}}^{\text{qh}}$ (see below), we employed a dense \mathbf{k} -point grid of $16 \times 16 \times 16$ for BZ integration. With these settings we found that the calculated quasi-harmonic free energies were accurate to within 5 meV per formula unit.

C. Free energy calculations

We computed the quasi-harmonic Gibbs free energy associated with the formation of neutral oxygen vacancies, $G_{\text{vac}}^{\text{qh}}$, as a function of epitaxial strain, $\eta \equiv (a - a_0)/a_0$ (where a_0 represents the equilibrium in-plane lattice parameter calculated for the stoichiometric system), and temperature, T , by following the approach introduced in previous works [25, 41]. Next, we briefly summarize the key aspects and technical details of the employed quasi-harmonic Gibbs free energy calculation method.

The formation Gibbs free energy of non-magnetic and neutrally charged V_{O} can be expressed as [25, 41]:

$$G_{\text{vac}}^{\text{qh}}(\eta, T) = E_{\text{vac}}(\eta) + F_{\text{vac}}^{\text{qh}}(\eta, T) + \mu_{\text{O}}(T), \quad (2)$$

where subscript “vac” indicates the quantity difference between the off-stoichiometric and stoichiometric systems (e.g., $E_{\text{vac}} \equiv E_{\text{SrTiO}_{3-\delta}} - E_{\text{SrTiO}_3}$), E_{vac} accounts

for the static contributions to the free energy (i.e., calculated at $T = 0$ conditions by considering the atoms fixed at their equilibrium lattice positions [8]), $F_{\text{vac}}^{\text{qh}}$ for the vibrational contributions to the free energy, and μ_{O} is the chemical potential of free oxygen atoms. The vibrational free energy of stoichiometric and off-stoichiometric systems were estimated with the quasi-harmonic formula [49–53]:

$$F^{\text{qh}}(\eta, T) = \frac{1}{N_q} k_B T \sum_{\mathbf{q}_s} \ln \left[2 \sinh \left(\frac{\hbar \omega_{\mathbf{q}_s}(\eta)}{2k_B T} \right) \right], \quad (3)$$

where N_q is the total number of wave vectors used for integration within the Brillouin zone and the dependence of the phonon frequencies, $\omega_{\mathbf{q}_s}$, on epitaxial strain is explicitly noted.

It is well known that first-principles estimation of μ_{O} with DFT+ U methods is challenging and may lead to large errors [54, 55]. Such inherent limitations make the prediction of V_{O} formation energies by exclusively using DFT approaches difficult and probably also imprecise. Notwithstanding, since (i) the oxygen chemical potential does not depend on epitaxial strain (i.e., in practice the value of μ_{O} is determined by the experimental conditions) and (ii) our main aim is to unravel the impact of lattice excitations on the formation energy and diffusion of V_{O} as a function of η , we can safely base our analysis on the results obtained for the thermodynamically shifted Gibbs free energy:

$$G_{\text{vac}}^{*\text{qh}}(\eta, T) = G_{\text{vac}}^{\text{qh}}(\eta, T) - \mu_{\text{O}}(T). \quad (4)$$

In other words, rather than adopting experimental values for μ_{O} and/or applying empirical corrections to the calculated vacancy formation energies [40, 55], we select arbitrary values for the oxygen-gas chemical potential without any loss of generality.

D. Nudged elastic band calculations

Ab initio nudged-elastic band (NEB) calculations [56] were performed to estimate the activation energy for V_{O} diffusion in epitaxially strained (001) SrTiO_3 at zero temperature. Our NEB calculations were performed for reasonably large $2 \times 2 \times 2$ or $3 \times 3 \times 3$ supercells containing several tens of atoms [46]. We used \mathbf{q} -point grids of $8 \times 8 \times 8$ or $6 \times 6 \times 6$ and an energy plane-wave cut-off of 650 eV. Six intermediate images were used to determine the most likely V_{O} diffusion paths in the absence of thermal excitations. The geometry optimizations were halted when the total forces on the atoms were smaller than $0.01 \text{ eV} \cdot \text{\AA}^{-1}$. The NEB calculations were performed for five epitaxial-strain equidistant points in the interval $-4 \leq \eta \leq 4\%$.

E. *Ab initio* molecular dynamics simulations

First-principles molecular dynamics (AIMD) simulations based on DFT were performed in the canonical (N, V, T) ensemble. The selected volumes and geometries were those determined at zero-temperature conditions, hence we neglected thermal expansion effects. The concentration of oxygen vacancies in the off-stoichiometric systems was also considered to be independent of T and equal to $\approx 1.6\%$. The temperature in the AIMD simulations was kept fluctuating around a set-point value by using Nose-Hoover thermostats. Large simulation boxes containing 317 atoms ($\text{Sr}_{64}\text{Ti}_{64}\text{O}_{189}$) were employed in all the AIMD simulations and periodic boundary conditions were applied along the three Cartesian directions. Newton's equation of motion were integrated by using the customary Verlet's algorithm and a time-step length of $\delta t = 10^{-3}$ ps. Γ -point sampling for integration within the first Brillouin zone was employed in all the AIMD simulations. The calculations comprised total simulation times of $t_{\text{total}} \sim 10$ ps. We performed three AIMD simulations at $T = 1000, 1500,$ and 2000 K for off-stoichiometric STO thin films considering epitaxial strains of $-3.6, 0$ and $+3.6\%$.

The mean square displacement (MSD) of oxygen ions was estimated with the formula [57]:

$$\text{MSD}(\tau) = \frac{1}{N_{\text{ion}} (N_{\text{step}} - n_{\tau})} \times \sum_{i=1}^{N_{\text{ion}}} \sum_{j=1}^{N_{\text{step}} - n_{\tau}} |\mathbf{r}_i(t_j + \tau) - \mathbf{r}_i(t_j)|^2, \quad (5)$$

where $\mathbf{r}_i(t_j)$ is the position of a migrating ion i at time t_j ($= j \cdot \delta t$), τ represents a lag time, $n_{\tau} = \tau/\delta t$, N_{ion} is the total number of mobile ions, and N_{step} the total number of time steps. The maximum n_{τ} was chosen equal to $N_{\text{step}}/3$ (i.e., equivalent to $\sim 3\text{--}4$ ps), hence we could accumulate enough statistics to reduce significantly the MSD(τ) fluctuations at the largest τ (see the error bars in the MSD plots presented in the following sections). Oxygen diffusion coefficients were subsequently obtained with the Einstein relation:

$$D = \lim_{\tau \rightarrow \infty} \frac{\text{MSD}(\tau)}{6\tau}. \quad (6)$$

The T -dependence of the oxygen diffusion coefficient was assumed to follow the Arrhenius formula:

$$D(T) = D_0 \cdot \exp \left[-\frac{E_a}{k_B T} \right], \quad (7)$$

where D_0 is known as the pre-exponential factor, E_a is the activation energy for ionic diffusion, and k_B the Boltzmann constant.

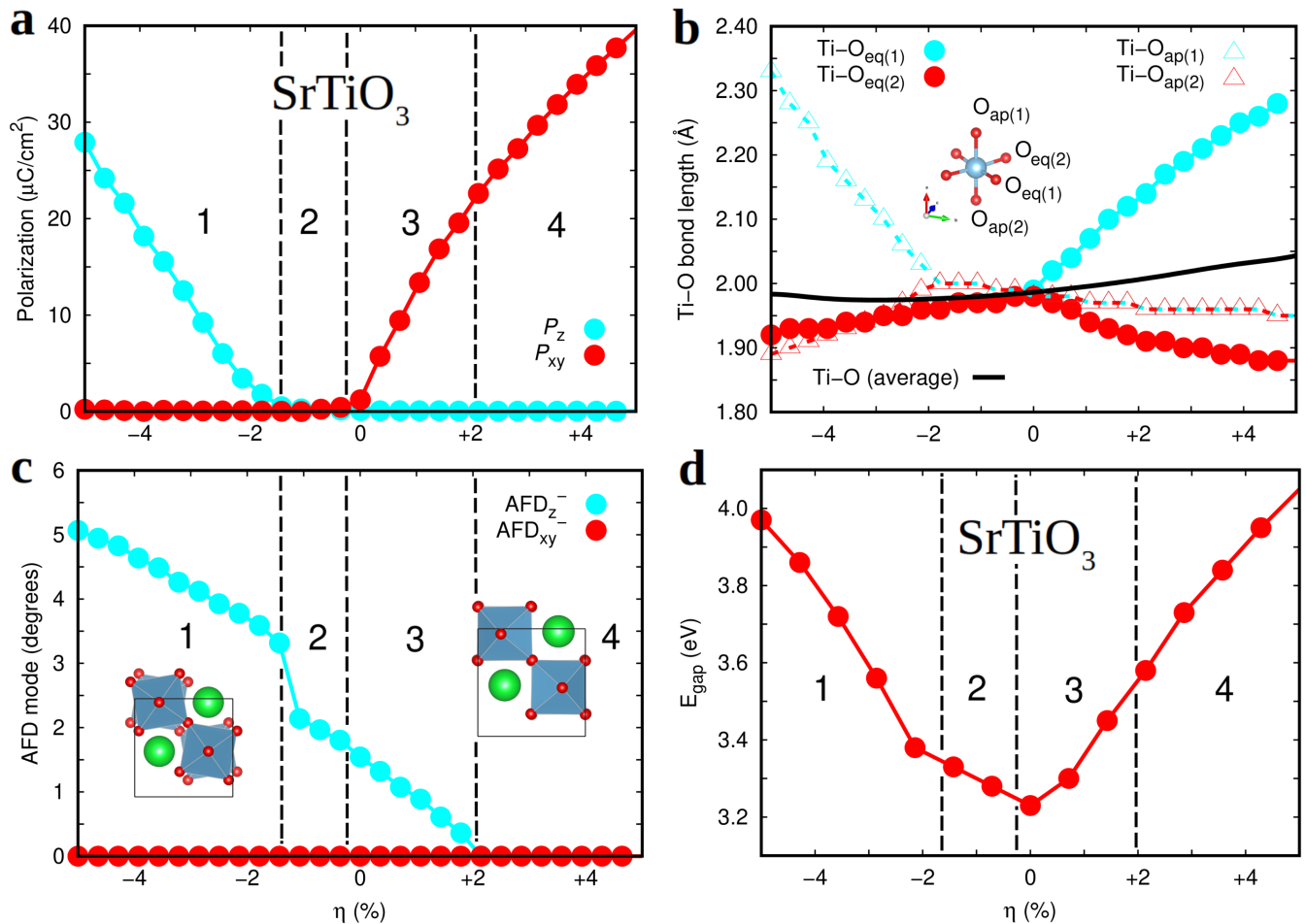


FIG. 2: Physical properties of stoichiometric (001) SrTiO₃ thin films estimated with first-principles methods. **a** The electric polarization along the out-of-plane (P_z) and in-plane (P_{xy}) directions expressed as a function of epitaxial strain, η . **b** Different Ti-O bond lengths expressed as a function of epitaxial strain. **c** Antiferrodistortive O₆ rotations expressed as a function of epitaxial strain. **d** Energy band gap of (001) SrTiO₃ thin films estimated with the range-separated hybrid functional HSE06 [58] on the geometries determined at the PBE+ U level. The vertical lines indicate different phase stability regions, namely, 1. $I4cm$, 2. $I4/mcm$, 3. $Ima2$ and 4. $Amm2$.

III. RESULTS AND DISCUSSION

We start by discussing the zero-temperature phase diagram of stoichiometric (001) STO thin films calculated with first-principles methods. The changes in the structural and electric polarization properties induced by the presence of equatorial (Eq) and apical (Ap) oxygen vacancies (V_{O}) are subsequently explained. The impact of thermal effects on the formation energy of V_{O} is analyzed for a wide range of epitaxial strain (η) and temperature conditions. We also report and compare the energy barriers for ionic oxygen diffusion in (001) STO thin films estimated by neglecting and by taking into account T -induced lattice vibrations. Insightful connections between our theoretical results and experimental measurements are provided whenever the latter are available in the literature.

A. Zero-temperature properties of stoichiometric (001) SrTiO₃ thin films

Figure 2 shows the structural, electric polarization and energy band gap properties of stoichiometric (001) SrTiO₃ thin films estimated with first-principles methods (i.e., density functional theory –DFT–, Sec. II) at zero temperature. Different crystalline phases are stabilized as a result of varying the epitaxial strain conditions, which are described in detail next. We note that several authors have previously reported analogous DFT results to ours [15, 59–61] and that the best agreement with the present calculations is obtained for work [61], in which antiferrodistortive oxygen octahedra rotations (AFD) were also explicitly modeled.

In the epitaxial strain interval $\eta \lesssim -2\%$, we observe the stabilization of a tetragonal $I4cm$ phase that is characterized by a significant out-of-plane polarization (P_z ,

Fig.2a) and antiphase out-of-plane O_6 rotations (AFD_z^- , Fig.2c). Coexistence of the order parameters P_z and AFD_z^- is quite unique as they normally tend to oppose each other [31], a polar-antiferrodistortive interplay that has been experimentally observed and characterized as a function temperature and η [30]. Under tensile strain, half of the Ti–O bond lengths involving oxygen atoms in apical positions are significantly elongated as compared to those involving O ions in equatorial positions (Fig.2b), a structural distortion that signals the presence of out-of-plane polarization [16, 18].

In the epitaxial strain interval $-2 \lesssim \eta \lesssim 0\%$, a tetragonal $I4/mcm$ phase appears that presents null electric polarization (Fig.2a) and moderate antiphase out-of-plane O_6 rotations (Fig.2c). In this phase, the length of the Ti–O bonds are all pretty similar regardless of the positions occupied by the oxygen atoms (Fig.2b). It is worth noting that when some tiny monoclinic lattice distortions in the generated equilibrium geometries (i.e., $\alpha \sim 0.1$ degrees) are not disregarded the identification of this phase is also compatible with a non-polar $C2/c$ phase that is similar to the one previously predicted for metallic $LaNiO_3$ thin films [62].

In the epitaxial strain interval $0 \lesssim \eta \lesssim +2\%$, a noticeable in-plane electric polarization, P_{xy} , appears in the system that coexists with small AFD_z^- O_6 rotations (Fig.2a,c). The resulting crystal phase is orthorhombic and its symmetry can be ascribed to the polar space group $Ima2$. Under tensile strain, half of the Ti–O bond lengths involving oxygen atoms in equatorial positions are significantly elongated as compared to those involving O ions in apical positions (Fig.2b), a structural distortion that produces a significant in-plane polarization [16, 18]. In the epitaxial strain interval $\eta \gtrsim +2\%$, the antiphase out-of-plane O_6 rotations completely disappear and P_{xy} grows steadily under increasing epitaxial strain. In this latter case, the optimized crystal structure is also orthorhombic and its symmetry can be identified with the space group $Amm2$.

Figure 2d shows the energy band gap of (001) $SrTiO_3$ thin films, E_{gap} , estimated as a function of epitaxial strain with the range-separated hybrid functional HSE06 [58]. The reason for including this information here will become clearer in the next subsection, where we explain the oxygen vacancy formation energy results obtained at zero temperature. It is worth noting that E_{gap} increases noticeably under either tensile or compressive biaxial strain as compared to the corresponding zero-strain value. For instance, at $\eta = 0$ the energy band gap amounts to 3.2 eV whereas at $\eta = \pm 4\%$ is approximately equal to 3.9 eV. Such a η -induced E_{gap} trend is markedly different from the one predicted for binary oxides like CeO_2 and TiO_2 by using analogous first-principles methods [21], which displays a significant E_{gap} reduction under tensile biaxial strain. The reason for such a difference in E_{gap} behaviour is likely to be related to the larger changes in the dielectric susceptibility that can be induced by epitaxial strain in STO thin films as compared

to binary oxides [21, 59].

B. Formation energy of oxygen vacancies at $T = 0$

Figure 3 shows the formation energy of oxygen vacancies calculated for (001) STO thin films at zero temperature, E_{vac} . The concentration of V_O considered in this case renders the composition $SrTiO_{2.75}$ (analogous vacancy energy results obtained for smaller oxygen vacancy concentrations are explained below). A small decrease in E_{vac} is observed as the biaxial strain changes from compressive to tensile (i.e., of $> 1\%$ when considering the two limiting cases $\eta = \pm 4\%$, Fig.3a). For most η cases, it seems more favourable to create apical V_O than equatorial, however the formation energy differences between the two cases are pretty small (i.e., $|\Delta E_{vac}| \approx 0.01$ eV per formula unit, Fig.3a).

For negative η values, the creation of oxygen vacancies in either equatorial (Fig.3c) or apical (Fig.3d) positions has a dramatic effect on the electric polarization of the system. In particular, the sizable out-of-plane polarization found in stoichiometric STO thin films (Fig.2a) practically disappears when V_O are exclusively created in apical positions. Meanwhile, when oxygen vacancies are generated solely in equatorial positions a non-negligible in-plane polarization of $\approx 7 \mu C cm^{-2}$ appears for any value of compressive epitaxial strain. For positive η values, on the other hand, the general behaviour of the electrical polarization is quite similar to that found for the analogous stoichiometric thin films, although the size of P_{xy} appreciably decreases ($\sim 10\%$).

Figure 3b shows the volume difference between $SrTiO_{2.75}$ and stoichiometric thin films, ΔV_{vac} , expressed as a function of epitaxial strain. The creation of neutral oxygen vacancies in oxide perovskites typically induces an increase in volume, the so-called chemical expansion, due to the electronic reduction of transition metal ions that are located close to V_O 's [41, 63]. For present purposes, it is interesting to analyze the η -dependence of ΔV_{vac} because this quantity has been found to be correlated with the contribution of lattice thermal excitations to the formation energy of V_O at finite temperatures [41]. As regards equatorial oxygen vacancies, ΔV_{vac} turns out to be positive and moderately large (small) under tensile (compressive) epitaxial strain. By contrast, the creation of apical oxygen vacancies is accompanied by negative (positive) and large ΔV_{vac} absolute values (small) at large compressive (tensile) epitaxial strain (Fig.3b). In the next subsection, we will comment on possible correlations between these zero-temperature ΔV_{vac} results and the lattice-related contributions to the formation energy of V_O at finite temperatures (i.e., the Gibbs free energy G_{vac}^{*qh} shown in Eq.(4)).

The estimation of oxygen vacancy formation energies may depend strongly on the concentration of V_O considered in the simulations due to the presence of short- and long-ranged interactions acting between the defects

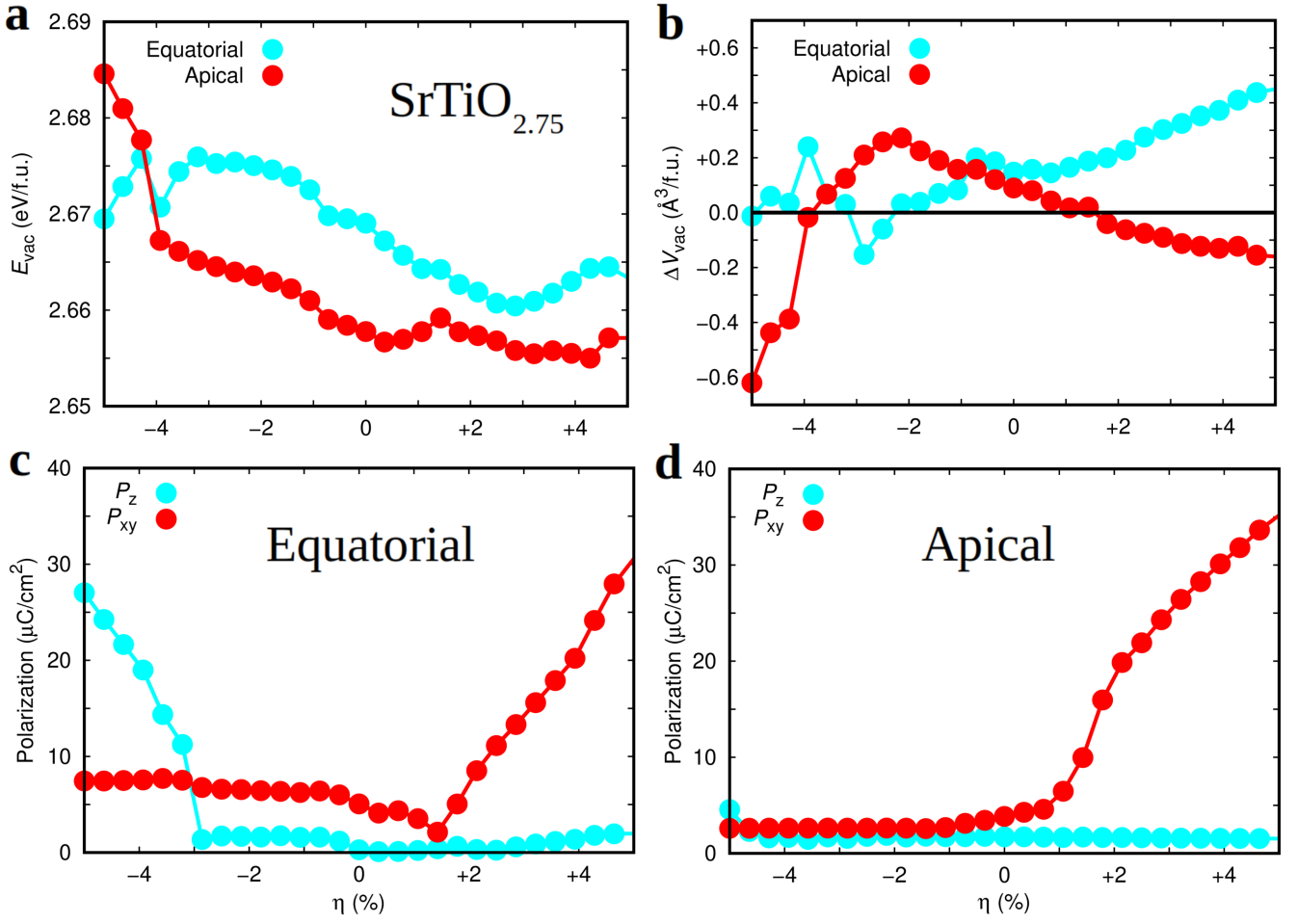


FIG. 3: Zero-temperature properties of non-stoichiometric epitaxially strained (001) $\text{SrTiO}_{2.75}$ estimated with first-principles methods based on DFT (Sec. II). **a** Zero-temperature formation energy of oxygen vacancies expressed as a function of oxygen position and epitaxial strain. **b** Volume change per formula unit, $\Delta V_{\text{vac}} \equiv V_{\text{SrTiO}_{2.75}} - V_{\text{SrTiO}_3}$, induced by the creation of oxygen vacancies and expressed as a function of oxygen position and epitaxial strain. The electric polarization along the out-of-plane (P_z) and in-plane (P_{xy}) directions expressed as a function of epitaxial strain for (001) $\text{SrTiO}_{2.75}$ thin films containing **c** equatorial and **d** apical oxygen vacancies.

[2, 8]. Figures 3a and 4 explicitly show this effect, as it is found that by decreasing the V_{O} concentration the computed zero-temperature formation energy dramatically decreases for any arbitrary value of η . For instance, the estimated E_{vac} for unstrained $\text{SrTiO}_{2.75}$ and $\text{SrTiO}_{2.94}$ amounts to 2.7 and 0.6 eV, respectively. This result suggests that short and middle-range interactions between oxygen vacancies are of repulsive type and thus the formation of V_{O} clusters in STO thin films in principle is not likely to occur at low and moderate temperatures. Moreover, the E_{vac} difference between equatorial and apical oxygen vacancies also depends critically on the concentration of defects. Specifically, according to our E_{vac} results obtained for $\text{SrTiO}_{2.75}$ thin films in general it is more favourable to create apical V_{O} than equatorial (Fig.3a) whereas for $\text{SrTiO}_{2.94}$ thin films the tendency is just the opposite (Fig.4b). The effect of epitaxial strain on E_{vac} also varies as the concentration of

V_{O} changes. In particular, E_{vac} increases both under compressive and tensile strains for $\text{SrTiO}_{2.94}$ thin films whereas for $\text{SrTiO}_{2.75}$ it decreases under tensile strain.

How do these zero-temperature V_{O} formation energy results compare with the available experimental data? In a recent paper, Rivadulla and collaborators have measured the enthalpy of oxygen vacancy formation for STO thin films as a function of epitaxial stress [34]. The authors have found that under both compressive and tensile strains such energy noticeably decreases. For instance, in the experiments the V_{O} formation enthalpy decreases by $\approx 20\%$ ($\approx 40\%$) for a tensile (compressive) strain of 1% as compared to the unstrained case [34]. Therefore, the agreement between our zero-temperature E_{vac} results expressed as a function of η and V_{O} concentration (Figs.3a,4) and the experimental observations is far from satisfactory. In order to fundamentally understand the origins of such large discrepancies, and based on the fact

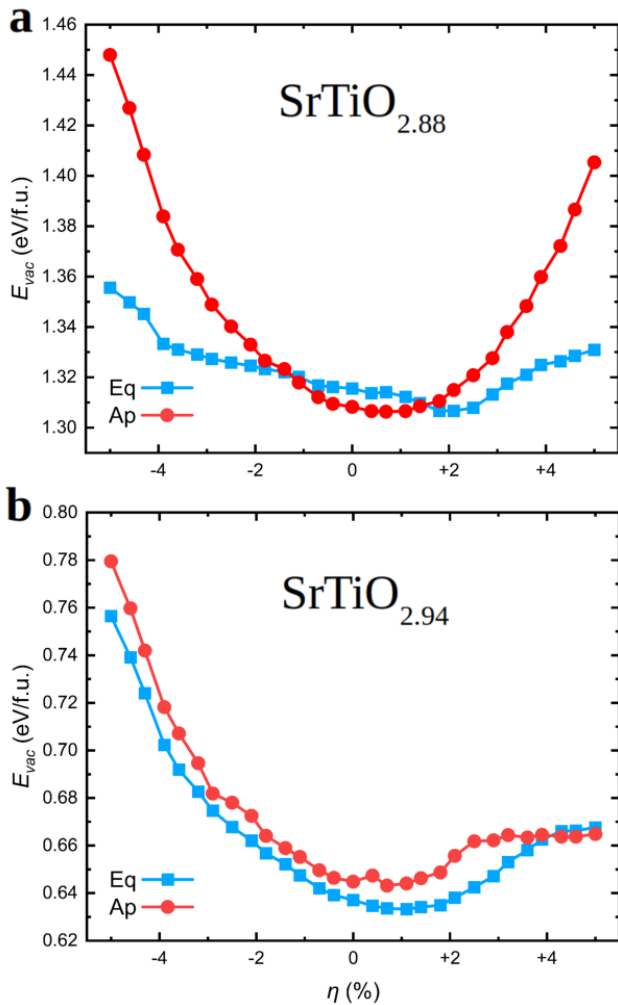


FIG. 4: Zero-temperature formation energy of oxygen vacancies expressed as a function of oxygen position and epitaxial strain for compositions **a** $\text{SrTiO}_{2.88}$ and **b** $\text{SrTiO}_{2.94}$. Labels “Eq” and “Ap” stand out for equatorial and apical V_O , respectively.

that oxygen vacancies in oxide perovskites typically are created at high temperatures [7, 25, 34], we proceeded to explicitly calculate V_O formation free energies at finite temperatures (rather than at non-realistic $T = 0$ conditions).

Before explaining our V_O formation energy results obtained at $T \neq 0$ conditions, it is worth mentioning that in a recent work [33] another first-principles study on the V_O formation energy of STO thin films has been reported. Zero-temperature E_{vac} results analogous to ours are presented in [33], however, the conclusions reported in that study are drastically different from the computational outcomes just described in this section. In particular, a systematic decrease in E_{vac} has been predicted for either tensile or compressive strains, which is the opposite behaviour than what we have found here for $\text{SrTiO}_{2.94}$ thin films, for instance. Moreover, an intriguing corre-

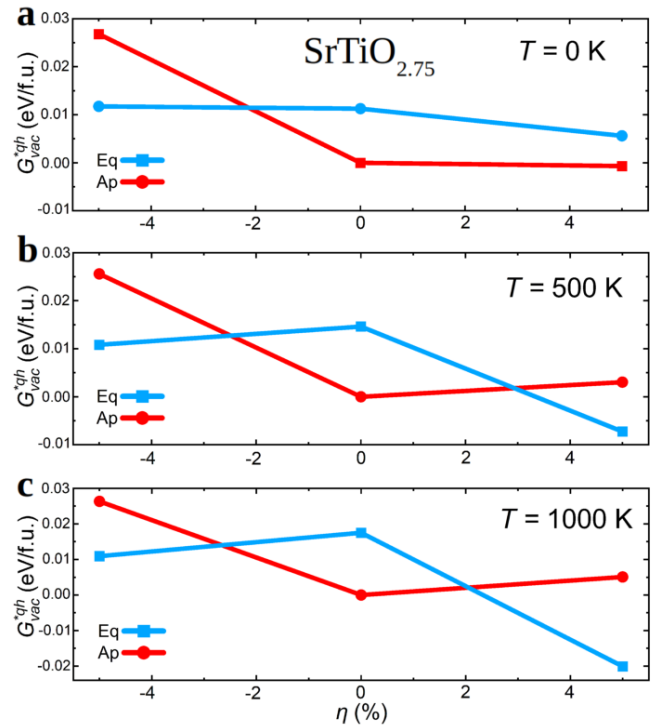


FIG. 5: Thermodynamically μ_O -shifted Gibbs free energy [Eqs.(2)–(4)] (Sec. II C) for V_O formation expressed as a function of oxygen vacancy position, epitaxial strain and temperature. **a** $T = 0$ K, **b** $T = 500$ K, and **c** $T = 1000$ K. The composition of the off-stoichiometric (001) thin films corresponds to $\text{SrTiO}_{2.75}$ and labels “Eq” and “Ap” stand out for equatorial and apical oxygen vacancies, respectively.

lation between the η -induced behaviour of E_{vac} and the energy band gap of STO thin films (E_{gap}) has been also suggested in work [33]. Based on our results enclosed in Figs.2d and 4b, such a correlation is partially corroborated [21]. Nevertheless, in our calculations both quantities E_{vac} and E_{gap} increase, rather than decrease, under either tensile or compressive strains. We hypothesize that the likely reasons for such theoretical disagreements may be the neglect of characteristic STO structural motifs in work [33], like polar and antiferrodistortive oxygen octahedral distortions.

C. Formation energy of oxygen vacancies at $T \neq 0$

We performed quasi-harmonic Gibbs free energy calculations to estimate the formation energy of oxygen vacancies at finite temperatures, G_{vac}^{*qh} [Eq.(4)], for epitaxially constrained (001) $\text{SrTiO}_{2.75}$ thin films using the methods explained in Sec.II C. Unfortunately, due to the huge computational effort associated with the calculation of phonon spectra of off-stoichiometric systems, we could not assess the dependence of G_{vac}^{*qh} on the concentration of V_O . Figure 5 shows our G_{vac}^{*qh} results expressed as a function of temperature and epitaxial strain. Since

here we are primarily interested in analyzing the joint effects of epitaxial strain and lattice thermal excitations on the formation energy of oxygen vacancies, the chemical potential entering Eq.(4) has been arbitrarily selected, without any loss of generality, to provide null $G_{\text{vac}}^{*\text{qh}}$ values for the minimum energy determined under $\eta = 0$ conditions at each temperature.

We found that lattice thermal excitations hardly affect the μ_{O} -shifted formation energy of apical V_{O} 's, independently of the epitaxial strain. In particular, only a small $G_{\text{vac}}^{*\text{qh}}$ increase of few meV per formula unit is appreciated under tensile strain as compared to the values estimated at zero temperature (Figs.5a,c). By contrast, the η -dependence of the μ_{O} -shifted formation energy of equatorial V_{O} 's drastically changes as a result of considering T -induced lattice vibrations. For instance, at the highest analyzed temperature, $T = 1000$ K, $G_{\text{vac}}^{*\text{qh}}$ decreases by as much as $\approx 50\%$ for a biaxial strain of -5% and by $\approx 200\%$ for $\eta = +5\%$ (Fig.5c). For an intermediate temperature of 500 K, the observed tendency is analogous to the one just described although the $G_{\text{vac}}^{*\text{qh}}$ differences with respect to the unstrained case are slightly smaller (i.e., a reduction of $\approx 35\%$ and $\approx 150\%$ for $\eta = -5$ and $+5\%$, respectively –Fig.5b–).

The differences between the estimated $G_{\text{vac}}^{*\text{qh}}$ as a function of T and η for apical and equatorial V_{O} can be qualitatively understood in terms of the zero-temperature proxy ΔV_{vac} introduced in Sec.III B (Fig.3b). In a recent theoretical paper [41], it has been proposed that for positive ΔV_{vac} values, that is, $V_{\text{SrTiO}_{3-\delta}} > V_{\text{SrTiO}_3}$, lattice thermal excitations tend to facilitate the formation of oxygen vacancies. As it is observed in Fig.3b, for equatorial vacancies ΔV_{vac} is positive and steadily increases under tensile biaxial strain; this outcome is agreeing with the large relative $G_{\text{vac}}^{*\text{qh}}$ decrease estimated for $\eta = +5\%$ upon increasing temperature (Fig.5). Meanwhile, for apical vacancies ΔV_{vac} is negative under both large tensile and compressive strains; this behaviour is consistent with the fact that under increasing temperature the corresponding relative $G_{\text{vac}}^{*\text{qh}}$ differences hardly change. Therefore, we corroborate the previously proposed qualitative correlation between the two quantities ΔV_{vac} and $F_{\text{vac}}^{\text{qh}}$ (Sec.II C), which are computed at zero temperature and $T \neq 0$ conditions, respectively [41].

How do these finite-temperature V_{O} formation energy results compare with the experimental data reported in work [34]? The answer is that although the agreement between theory and observations is not quantitative it can be regarded as qualitatively satisfactory. We recall that experimentally it has been determined that under both compressive and tensile biaxial strains oxygen vacancies can be created more easily. This behaviour is analogous to what we have predicted for equatorial V_{O} 's, which in oxide perovskites correspond to the most representative class of anion positions (i.e., equatorial O sites are 50% more numerous than apical). Moreover, since the $G_{\text{vac}}^{*\text{qh}}$ values estimated for equatorial V_{O} 's under both tensile and compressive biaxial strains are smaller than those es-

timated for apical vacancies (by ≈ 30 and 20 meV per formula unit, respectively), it is likely that to a certain extent vacancy ordering occurs in epitaxially strained STO thin films (as it has been experimentally shown for grain boundaries in bulk STO from scanning transmission electron microscopy measurements [64]). On the down side, experiments indicate that it is more easy to create oxygen vacancies under compressive strain than under tensile strain [34] while our calculations predict the opposite trend (Fig.5). Nonetheless, based on our computational E_{vac} and $G_{\text{vac}}^{*\text{qh}}$ results, it can be concluded that in order to reproduce the experimentally observed η -induced enhancement of V_{O} formation with theoretical *ab initio* methods it is necessary to explicitly consider vibrational lattice thermal excitations in the calculations.

D. Zero-temperature activation energy for oxygen diffusion

The diffusion of V_{O} 's in oxide perovskites is a key parameter for the design of ionic-based devices [65]. In recent atomic force microscopy experiments performed by Iglesias *et al.* [37], it has been shown that tensile biaxial strain produces a substantial increase in the diffusion of O ions in STO thin films. In particular, the room-temperature diffusion coefficient of oxygen atoms, D_{O} , roughly increases by a factor of 4 upon a tensile biaxial strain of $\approx +2\%$ [37]. For compressive tensile strains, on the other hand, the available experimental data is quite scarce. Nonetheless, measurements performed up to a η of $\approx -1\%$ appear to suggest an incipient reduction in D_{O} [37]. On this regard, first-principles analysis of ionic transport properties may be very useful as calculations are free of the technical problems found in the experimental synthesis of epitaxially grown thin films and thus arbitrarily large tensile/compressive biaxial strains can be simulated.

First-principles simulation of ionic diffusion processes, however, are neither exempt of some technical issues and shortcomings [57]. For instance, due to the intense computational expense associated with $T \neq 0$ simulations, most first-principles studies usually neglect temperature effects. In particular, zero-temperature calculations of ion-migration energy barriers typically are performed with the nudged elastic band (NEB) method [56] (Sec.III D), in which (i) the initial and final diffusion positions of the vacancy and interstitial ions need to be guessed in the form of high-symmetry configurations rendering metastable states, and (ii) T -induced lattice excitations are totally neglected. Limitations of the NEB method for accurately determining ionic diffusion energy barriers and paths are well known and documented for some prototype fast-ion conductor materials (e.g., see works [57] and [66]).

Al-Hamadany *et al.* have already studied the migration of oxygen vacancies in (001) STO thin films by means of NEB and DFT methods [38, 39]. For the case of ten-

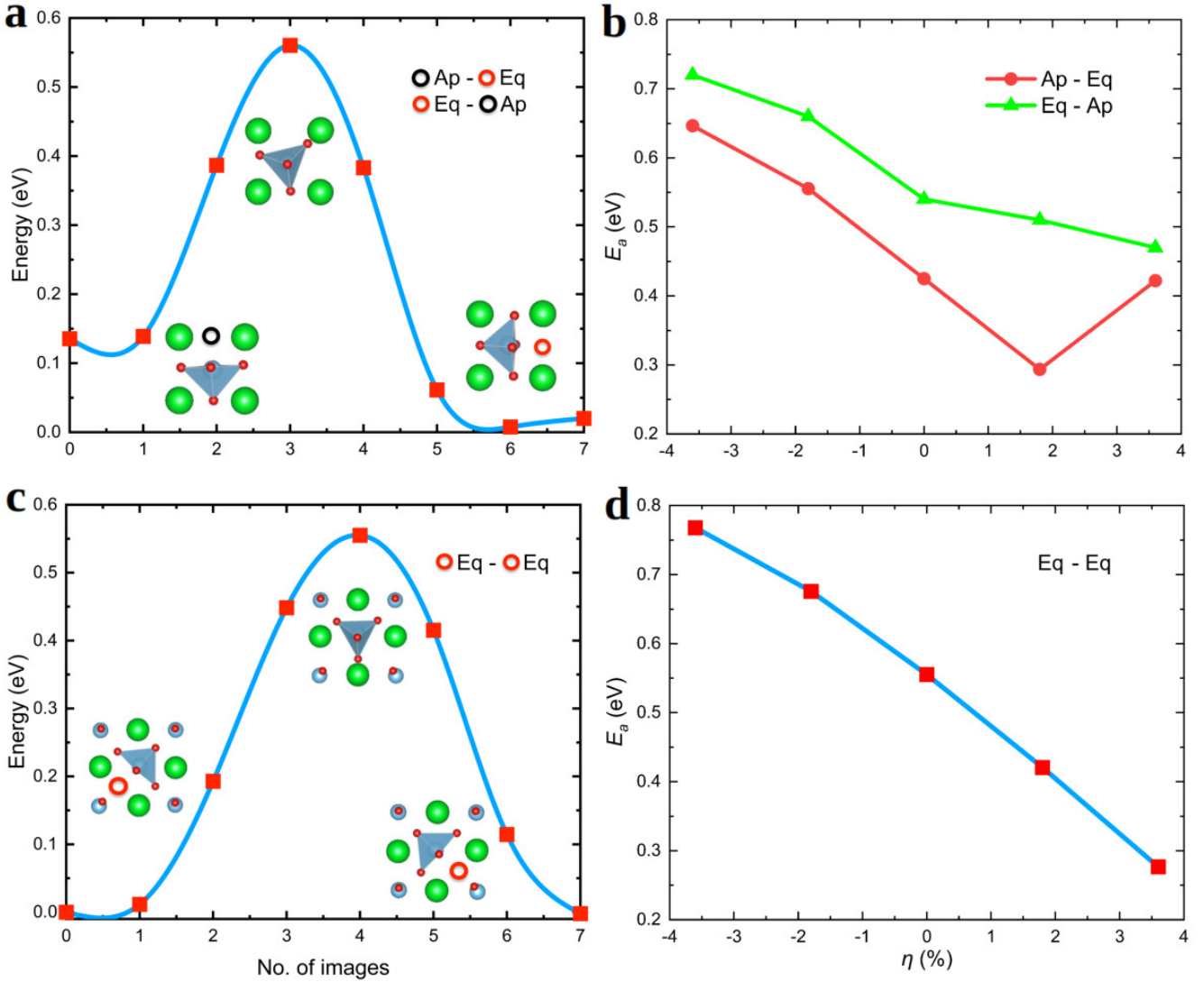


FIG. 6: Energy barriers for V_O diffusion calculated with the NEB method (Sec.IID) and by neglecting thermal lattice fluctuations. Representation of the analyzed oxygen vacancy diffusion paths are shown in **a** and **c** ($\eta = 0$ case). NEB energy barrier results expressed as a function of epitaxial strain are represented in **b** and **d**. Labels “Eq” and “Ap” stand out for equatorial and apical oxygen vacancies, respectively. The colouring code for atoms in **a** and **c** coincides with that indicated in Fig.1.

sile biaxial strains, Al-Hamadany *et al.* have reported a systematic and significant reduction in the energy barrier for V_O diffusion, E_a (i.e., of up to 25% for large η 's of +6–8% [39]). This computational outcome is in good agreement with the experimental tendency found by Iglesias *et al.* for D_O [37]. The value of the reported NEB activation energy calculated at zero-strain conditions is approximately 0.8 eV. For the case of compressive biaxial strains, Al-Hamadany *et al.* have also reported a decrease in E_a for high $|\eta|$'s of $> 4\%$ [38] (i.e., of up to 50% for η 's of $-6-8\%$); in the $0 \leq \eta \leq 4$ interval, on the other hand, the energy barrier for V_O diffusion hardly changes or increases just moderately (depending on the considered initial and final oxygen vacancy positions).

Figure 6 shows our E_a results obtained for (001) STO thin films by employing DFT NEB techniques

(Sec.IIID). Two possible V_O diffusion paths, namely, “Ap-Eq” (Fig.6a) and “Eq-Eq” (Fig.6c) where “Ap” and “Eq” stand for apical and equatorial O sites, have been considered in our simulations. In the former case, we obtain two different energy barriers, “Ap-Eq” and “Eq-Ap”, due to the energy asymmetry between the two involved oxygen positions (Figs.3 and 4). In consistent agreement with the available experimental data and previous DFT studies, we find that under tensile biaxial strain the energy barrier for V_O diffusion is greatly reduced. For instance, at $\eta \approx +4\%$ we obtain that E_a decreases with respect to the value estimated at zero strain (i.e., 0.55 eV) by $\approx 50\%$ and 15% for “Eq-Eq” (Fig.6d) and “Eq-Ap” (Fig.6b), respectively. (The V_O diffusion energy barrier difference between cases “Eq-Ap” and “Ap-Eq” simply correspond to the zero-temperature V_O for-

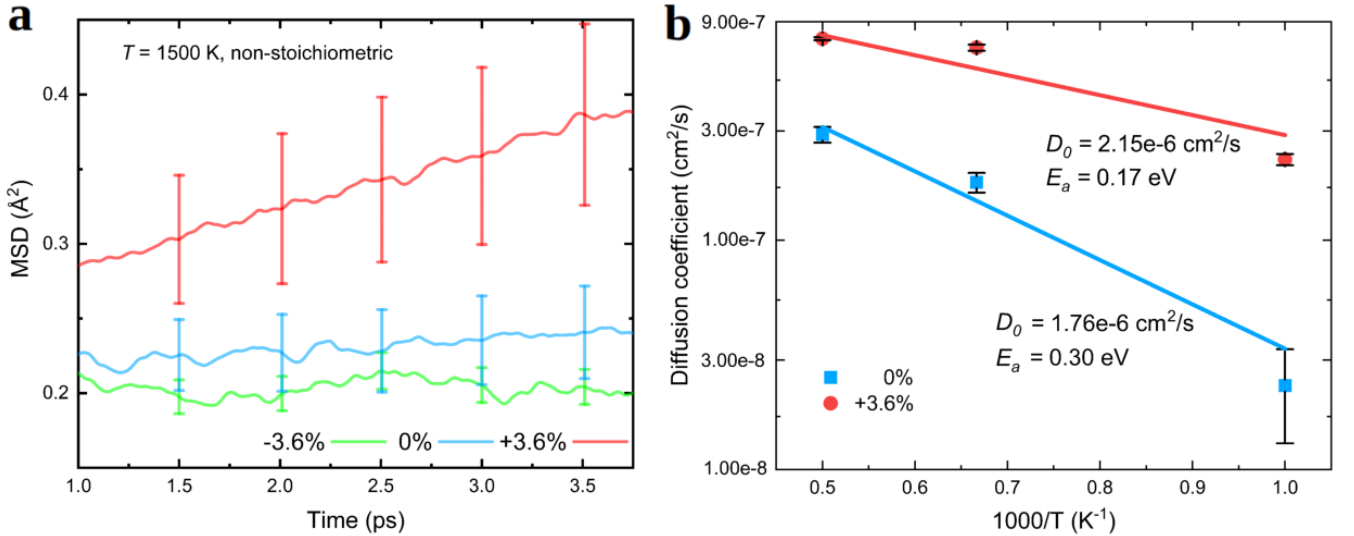


FIG. 7: **a** Mean square displacement (MSD) calculated for oxygen ions in off-stoichiometric (001) STO thin films with AIMD simulations performed at $T = 1500$ K and considering different epitaxial strain conditions, namely, $\eta = -3.6, 0$ and $+3.6\%$. **b** Oxygen diffusion coefficients estimated for off-stoichiometric (001) STO thin films with AIMD simulations considering different temperatures and epitaxial strain conditions. The resulting pre-exponential factors, D_0 , and activation energies, E_a , for oxygen ionic diffusion are indicated in the plot (Sec.IIE).

mation energy difference between cases “Eq” and “Ap”.) It is worth noting that our estimated zero-strain E_a value of 0.55 eV is in very good agreement with the experimental V_O diffusion energy barrier measured for bulk STO, $E_a^{\text{expt}} \approx 0.60$ eV [67].

Upon compressive biaxial strain, we find that E_a increases significantly and practically linearly with $|\eta|$ (Fig.6b,d). For instance, at $\eta \approx -4\%$ we predict that E_a increases with respect to the zero-strain value of 0.55 eV by $\approx 45\%$ and 32% for “Eq-Eq” (Fig.6d) and “Eq-Ap” (Fig.6b), respectively. These results appear to be in agreement with the scarce experimental data that is available for compressive biaxial strains [37] but in clear disagreement with previous DFT results reported by Al-Hamadany *et al.* [38]. The reasons for the disagreements between our theoretical NEB E_a estimations and others [38] are not clear to us since the distinctive structural motifs of STO thin films (e.g., polar and antiferrodistortive oxygen octahedral distortions) were considered in all works. In order to fully test the reliability of our E_a zero-temperature NEB results, we performed complementary *ab initio* molecular dynamics (AIMD) simulations in which lattice thermal excitations are fully taken into account and no particular V_O diffusion path needs to be guessed [57].

E. Oxygen ionic diffusion at finite temperature

Figure 7 encloses the MSD and D_O results obtained from our $T \neq 0$ AIMD simulations for (001) STO thin films at $\eta = \pm 3.6\%$ and zero strain (Sec.IIE). For the $\eta = 0$ case, we estimate large diffusion coefficients

of $\sim 10^{-8}$ – $10^{-7} \text{ cm}^2\text{s}^{-1}$ at temperatures higher than 1000 K and a small V_O diffusion energy barrier of 0.30 eV (Fig.7b). The pre-exponential factor entering the corresponding D_O Arrhenius formula (Sec.IIE) amounts to $1.8 \cdot 10^{-6} \text{ cm}^2\text{s}^{-1}$. The E_a value estimated by fully considering lattice thermal excitations is approximately 50% smaller than the one calculated with the NEB method considering zero-temperature conditions. This computational outcome demonstrates the existence of an important interplay between lattice vibrations and V_O diffusion, which in the case of STO thin films enormously facilitates ionic transport. It is also worth noting that the agreement between our zero-strain E_a result obtained from AIMD simulations and the experimental diffusion energy barrier $E_a^{\text{expt}} \approx 0.60$ eV [67] has considerably worsened as compared to the corresponding NEB estimation. Possible causes explaining such an extended disagreement could be the neglect of other types of defects in our $T \neq 0$ calculations, like dislocations [68], and the fact that the concentration of oxygen vacancies in our AIMD simulations ($\approx 1.6\%$) is probably larger than in the samples analyzed in the experiments.

For a tensile strain of $+3.6\%$, we find that the diffusion of oxygen vacancies is considerably enhanced as compared to the $\eta = 0$ case. In particular, we estimate high- T diffusion coefficients of $\sim 10^{-7} \text{ cm}^2\text{s}^{-1}$ and a reduced V_O diffusion energy barrier of 0.17 eV (Fig.7b). The value of the pre-exponential factor entering the corresponding D_O Arrhenius formula (Sec.IIE) is equal to $2.2 \cdot 10^{-6} \text{ cm}^2\text{s}^{-1}$. The E_a decrease induced by $\eta = +3.6\%$ is about 50% of the zero-strain value, which is very similar to the relative variation determined with NEB techniques for the same biaxial strain and “Eq-Eq” vacancy diffusion path

(Sec.IIID). In this case, it is also concluded that the effects of lattice thermal excitations is to significantly enhance oxygen transport.

As regards compressive biaxial strains, it is found that even at temperatures as high as 1500 and 2000 K the diffusion coefficient of oxygen atoms is nominally zero (Fig.7a). This AIMD result is in qualitative agreement with the NEB calculations presented in the previous section, since in the latter case we found that E_a increases almost linearly with $|\eta|$ (Sec.IIID). We note that if the energy barrier for V_O diffusion hardly changed under large compressive strains, then for $\eta = -3.6\%$ we would have estimated similar MSD and D_O values to those obtained for the unstrained system, which is not the case.

Overall, the AIMD simulation results presented in this section confirm the correctness (at the qualitative level) of our NEB results reported in Sec.IIID, and demonstrate that lattice thermal vibrations have a significant enhancing effect on V_O diffusion in (001) STO thin films. Interestingly, it is not always the case that lattice thermal excitations are found to promote ionic transport. For instance, in a recent systematic theoretical study on Li-based fast-ion conductors [57] the opposite trend has been demonstrated, namely, the energy barriers for ionic transport estimated from AIMD simulations in general are higher than those obtained with NEB methods. It is likely that the degree of anharmonicity of the non-diffusing lattice in the considered material, which determines the amplitude of the atomic fluctuations around the corresponding equilibrium positions, is directly related to the either enhancing or suppressing ionic diffusion effect mediated by the lattice excitations. Further quantitative investigations on this subject deserve future work.

IV. CONCLUSIONS

We have presented a comprehensive *ab initio* study on the formation energy and diffusion properties of oxygen

vacancies in epitaxially strained (001) STO thin films, a class of functional materials with great fundamental and applied interests. The novelty of our work lies in the incorporation of lattice thermal excitations on the first-principles description of V_O . It has been demonstrated that in order to achieve an improved agreement with the experimental observations it is necessary to explicitly consider temperature-induced lattice effects in the theoretical calculations. For instance, by performing quasi-harmonic Gibbs free energy calculations we have been able to qualitatively reproduce the nonmonotonic peak-like dependence of the V_O formation enthalpy measured in experiments. Also, by performing *ab initio* molecular dynamics simulations we have been able to reproduce the qualitative η -driven V_O diffusion trends observed in biaxially strained (001) STO samples. Generalization of our main conclusions to other technologically relevant oxide perovskite materials is likely, although further experimental and computational works on the interplay between oxygen vacancies and epitaxial strain are necessary. We hope that the present study will stimulate research efforts in this direction.

Acknowledgments

D.C. and C.C. acknowledge support from the Australian Research Council through funded projects LP190100113 and LP190100829. C.C. acknowledges support from the Spanish Ministry of Science, Innovation and Universities under the ‘‘Ram3n y Cajal’’ fellowship RYC2018-024947-I. Computational resources and technical assistance were provided by the Australian Government and the Government of Western Australia through Magnus under the National Computational Merit Allocation Scheme and The Pawsey Supercomputing Centre, and by the University of Valencia through the Tirant III cluster and its technical service.

-
- [1] S. S. Mofarah *et al.*, Adv. Mater. **31**, 1905288 (2019).
 - [2] S. S. Mofarah *et al.*, Nat. Commun. **10**, 2594 (2019).
 - [3] S. Kong, N. Kumar, S. Checchia, C. Cazorla, and J. E. Daniels, Adv. Funct. Mater. **29**, 1900344 (2019).
 - [4] C. Cazorla, M. V. Ganduglia-Pirovano, and J. Carrasco, Front. Chem. **7**, 547 (2019).
 - [5] M. V. Ganduglia-Pirovano, A. Hofmann, and J. Sauer, Surf. Sci. Rep. **62**, 219 (2007).
 - [6] X. Liu, K. Zhou, L. Wang, B. Wang, and Y. Li, J. Am. Chem. Soc. **131**, 3140 (2009).
 - [7] S. Hu, C. Cazorla, F. Xiang, H. Ma, J. Wang, J. Wang, X. Wang, C. Ulrich, L. Chen, and J. Seidel, ACS Appl. Mater. Interfaces **10**, 22348 (2018).
 - [8] C. Men3ndez, D. Chu, and C. Cazorla, npj Comput. Mater. **6**, 76 (2020).
 - [9] A. Lopez-Bezanilla, P. Ganesh, and P. B. Littlewood, Phys. Rev. B **92**, 115112 (2015).
 - [10] Y.-H. Huang, R. I. Dass, Z.-L. Xing, and J. B. Goodenough, Science **312**, 254 (2006).
 - [11] Y. Zhou, Z. Zhou, Y. Song, X. Zhang, F. Guan, H. Lv, Q. Liu, S. Miao, G. Wang, and X. Bao, Nano Energy **50**, 43 (2018).
 - [12] B. You, M. T. Tang, C. Tsai, F. Abild-Pedersen, X. Zheg, and H. Li, Adv. Mater. **31**, 1807001 (2019).
 - [13] W. Liang, Z. Zhuo, Y. Ji, C. Lu, M. Gao, H. Yang, C. Chen, F. Pan, and Y. Lin, npj Quantum Mater. **4**, 39 (2019).
 - [14] D. G. Schlom, L.-Q. Chen, C.-B. Eom, K. M. Rabe, S. K. Streiffer, and J.-M. Triscone, Annu. Rev. Mater. Res. **37**, 589 (2007).

- [15] T. Angsten, L. W. Martin, and M. Asta, *Phys. Rev. B* **95**, 174110 (2017).
- [16] C. Cazorla and M. Stengel, *Phys. Rev. B* **92**, 214108 (2015).
- [17] O. Diéguez and J. Íñiguez, *Phys. Rev. B* **95**, 085129 (2017).
- [18] C. Cazorla and M. Stengel, *Phys. Rev. B* **90**, 020101(R) (2014).
- [19] C. Escorihuela-Salayero, O. Diéguez, and J. Íñiguez, *Phys. Rev. Lett.* **109**, 247202 (2012).
- [20] Z. Shi, E. Tsymbalov, M. Dao, S. Suresh, S. Shapeev, and J. Li, *Proc. Natl. Acad. Sci. U. S. A.* **116**, 4117 (2019).
- [21] Z. Liu, J. Shenoy, C. Menéndez, J. N. Hart, C. C. Sorrell, C. Cazorla, *Nano Energy* **72**, 104732 (2020).
- [22] A. Kerklotz, D. Lee, E.-J. Guo, T. L. Meyer, J. R. Petrie, and H. N. Lee, *J. Phys.:Condens. Matter* **29**, 493001 (2017).
- [23] H. Jeen *et al.*, *Nat. Mater.* **12**, 1057 (2013).
- [24] J. R. Petrie *et al.*, *Adv. Funct. Mater.* **26**, 1564 (2016).
- [25] S. Hu, Y. Wang, C. Cazorla, and J. Seidel, *Chem. Mater.* **29**, 708 (2017).
- [26] K. A. Müller and H. Burkard, *Phys. Rev. B* **19**, 3593 (1979).
- [27] A. Ohtomo and H. Y. Hwang, *Nature* **427**, 423 (2004).
- [28] A. K. Yadav *et al.*, *Nature* **530**, 198 (2016).
- [29] J. H. Haeni *et al.*, *Nature* **430**, 758 (2004).
- [30] T. Yamada, B. W. Eerd, O. Sakata, A. K. Tagantsev, H. Morioka, Y. Ehara, S. Yasui, H. Funakubo, T. Nagasaki, and H. J. Trodahl, *Phys. Rev. B* **91**, 214101 (2015).
- [31] T. Gu, T. Scarbrough, Y. Yang, J. Íñiguez, L. Bellaiche, and H. J. Xiang, *Phys. Rev. Lett.* **120**, 197602 (2018).
- [32] M. Choi, F. Oba, Y. Kumagai, and I. Tanaka, *Adv. Mater.* **25**, 86 (2013).
- [33] S.-Y. Choi *et al.*, *Nano Lett.* **15**, 41219 (2015).
- [34] L. Iglesias, A. Sarantopoulos, C. Magén, and F. Rivadulla, *Phys. Rev. B* **95**, 165138 (2017).
- [35] Q. Yang, J. X. Cao, Y. Ma, Y. C. Zhou, L. M. Jiang, and X. L. Zhong, *J. Appl. Phys.* **113**, 184110 (2013).
- [36] Q. Yang, J. X. Cao, Y. C. Zhou, Y. Zhang, Y. Ma, and X. J. Lou, *Appl. Phys. Lett.* **103**, 142911 (2013).
- [37] L. Iglesias, A. Gómez, M. Gich, and F. Rivadulla, *ACS Appl. Mater. Interfaces* **10**, 35367 (2018).
- [38] R. Al-Hamadany, J. P. Gross, P. R. Briddon, S. A. Mojarad, M. Al-Hadidi, A. G. O'Neill, and M. J. Rayson, *J. Appl. Phys.* **113**, 024108 (2013).
- [39] R. Al-Hamadany, J. P. Gross, P. R. Briddon, S. A. Mojarad, A. G. O'Neill, and M. J. Rayson, *J. Appl. Phys.* **113**, 224108 (2013).
- [40] U. Aschauer, R. Pfenninger, S. M. Selbach, T. Grande, and N. A. Spaldin, *Phys. Rev. B* **88**, 054111 (2013).
- [41] C. Cazorla, *Phys. Rev. Appl.* **7**, 044025 (2017).
- [42] J. P. Perdew, K. Burke, and M. Ernzerhof, *Phys. Rev. Lett.* **77**, 3865 (1996).
- [43] G. Kresse and J. Fürthmüller, *Phys. Rev. B* **54**, 11169 (1996).
- [44] S. L. Dudarev, G. A. Botton, S. Y. Savrasov, C. J. Humphreys, and A. P. Sutton, *Phys. Rev. B* **57**, 1505 (1998).
- [45] P. E. Blöchl, *Phys. Rev. B* **50**, 17953 (1994).
- [46] L. Zhang, B. Liu, H. Zhuang, P. R. C. Kent, V. R. Cooper, and P. Ganesh, *Comput. Mater. Sci.* **118**, 309 (2016).
- [47] C. Menéndez and C. Cazorla, *Phys. Rev. Lett.* **125**, 117601 (2020).
- [48] D. Alfè, *Comp. Phys. Commun.* **180**, 2622 (2009).
- [49] C. Cazorla and J. Íñiguez, *Phys. Rev. B* **88**, 214430 (2013).
- [50] C. Cazorla, D. Errandonea, and E. Sola, *Phys. Rev. B* **80**, 064105 (2009).
- [51] C. Cazorla and J. Boronat, *Phys. Rev. B* **91**, 024103 (2015).
- [52] S. Baroni, P. Giannozzi, and E. Isaev, *Rev. Mineral. Geochem.* **71**, 39 (2010).
- [53] C. Cazorla and J. Boronat, *Rev. Mod. Phys.* **89**, 035003 (2017).
- [54] R. O. Jones and O. Gunnarsson, *Rev. Mod. Phys.* **61**, 689 (1989).
- [55] L. Wang, T. Maxisch, and G. Ceder, *Phys. Rev. B* **73**, 195107 (2006).
- [56] G. Henkelman, B. P. Uberuaga, and H. Jonsson, *J. Chem. Phys.* **113**, 9901 (2000).
- [57] A. K. Sagotra, D. Chu, and C. Cazorla, *Phys. Rev. Mater.* **3**, 035405 (2019).
- [58] J. Heyd, G. E. Scuseria, and M. Ernzerhof, *J. Chem. Phys.* **118**, 8207 (2003).
- [59] A. Antons, J. B. Neaton, K. M. Rabe, and D. Vanderbilt, *Phys. Rev. B* **71**, 024102 (2005).
- [60] C.-H. Lin, C.-M. Huang, and G. Y. Guo, *J. Appl. Phys.* **100**, 084104 (2006).
- [61] A. I. Lebedev, *Phys. Solid State* **58**, 300 (2016).
- [62] M. C. Weber *et al.*, *Phys. Rev. B* **94**, 014118 (2016).
- [63] D. Marrocchelli, N. H. Perry, and S. R. Bishop, *Phys. Chem. Chem. Phys.* **17**, 10028 (2015).
- [64] R. F. Klye, Y. Ito, S. Stemmer, and N. D. Browning, *Ultramicroscopy* **86**, 289 (2001).
- [65] T. Wan, B. Qu, H. Du, X. Lin, Q. Lin, D. Wang, C. Cazorla, S. Li, and D. Chu, *J. Colloid Interface Sci.* **512**, 767 (2018).
- [66] J. Yang and J. S. Tse, *J. Phys. Chem. A* **115**, 13045 (2011).
- [67] R. A. De Souza, V. Metlenko, D. Park, and T. E. Weirich, *Phys. Rev. B* **85**, 174109 (2012).
- [68] D. Marrocchelli, L. Sun, and B. Yildiz, *J. Am. Chem. Soc.* **137**, 4735 (2015).